

Observations of InSAR Closure Phase and Coherence Over Crops in the Thessaloniki Region, Greece

Lorette Drique, Manon Dalaison, Béatrice Pinel-Puysségur, Nobuaki Fuji

To cite this version:

Lorette Drique, Manon Dalaison, Béatrice Pinel-Puysségur, Nobuaki Fuji. Observations of InSAR Closure Phase and Coherence Over Crops in the Thessaloniki Region, Greece. 16th European Conference on Synthetic Aperture Radar, EUSAR 2026, Jun 2026, Baden - Baden, Germany. pp.104-109. ⟨hal-05762899⟩

HAL Id: hal-05762899

https://hal.science/view/index/docid/5762899

Submitted on 24 Sep 2026

HAL is a multi-disciplinary open access archive for the deposit and dissemination of scientific research documents, whether they are published or not. The documents may come from teaching and research institutions in France or abroad, or from public or private research centers.

L'archive ouverte pluridisciplinaire **HAL**, est destinée au dépôt et à la diffusion de documents scientifiques de niveau recherche, publiés ou non, émanant des établissements d'enseignement et de recherche français ou étrangers, des laboratoires publics ou privés.



Distributed under a Creative Commons CC BY-NC-SA 4.0 - Attribution - Non-commercial use - ShareAlike - International License

Observations of InSAR Closure Phase and Coherence Over Crops in the Thessaloniki Region, Greece

Lorette Drique[a,b], Manon Dalaison[a], Béatrice Pinel-Puysségur[b], and Nobuaki Fuji[a,c]
[a]Université Paris Cité, Institut de physique du globe de Paris, France
[b]CEA, DAM, DIF, F-91297 Arpajon, France
[c]Institut universitaire de France, Paris, France

Abstract

Land subsidence is occurring in the agricultural plain of Thessaloniki, Greece, and satellite Synthetic Aperture Radar interferometry (InSAR) provides a powerful means of measuring such deformation with high spatial resolution. However, variations in the backscattering properties of the surface, driven by changes in vegetation or soil moisture over cultivated areas, introduce decorrelation. Spatial filtering techniques, such as multilooking, can improve the signal-to-noise ratio in agricultural terrains; however, the resulting filtered signal contains cumulative phase errors that may bias deformation estimates. This bias manifests as a systematic non-zero closure phase over closed loops of multilooked interferograms. In this study, we investigate the influence of crops on coherence and closure phase in the region. Our analysis shows that coherence is anticorrelated with the rate of closure phase accumulation, although this relationship does not fully capture the observed variations. We further demonstrate that phase errors accumulate more rapidly over irrigated fields. By extracting seasonal patterns and comparing them with crop cycles, we find that the error exhibits a seasonal component following crop growth stages, which could be misinterpreted as ground deformation.

1 Introduction

Ground levelling and GPS measurements have revealed land subsidence in the Thessaloniki plains in Greece [1]. This is most likely due to the withdrawal of groundwater for crop irrigation [2]. Therefore, precise estimation of ground motion in the region can help to map land subsidence and provide information about groundwater storage variations, particularly in irrigated areas. This is of crucial importance for water management in this semi-arid climate.

Interferometric Synthetic Aperture Radar (InSAR) is widely employed to measure surface deformation from satellite observations, offering centimetre-level precision and temporal resolutions in the order of several days. However, changes in the backscattering properties of the ground can introduce cumulative errors in the measured interferometric phase that can be misinterpreted as deformation. The resulting bias in deformation timeseries can reach a few centimetres per year in vegetated regions, affecting all radar frequencies (C-band and L-band) [3]. Because the phase error associated with each interferogram, also called 'inconsistency' or 'fading signal', is poorly constrained mathematically, we quantify the closure phase, which is related to the phase errors of three interferograms in a closed loop [4].

The biased distribution of the phase error has been linked to different physical processes and is associated to non-zero closure phase. De Zan et al. [3] associate this error to the variable dielectric constant induced by soil moisture variations and the volume scattering linked to perpendicular spatial baseline and skewed vertical scattering profiles. Ansari et al. [4] show that soil-moisture-induced dielectric variations alone are unable to reproduce the full closure phase signal. The phase bias is expected to be greater on crops than on urban pixels [5]. Yuan et al. [6] show that considering the dielectric properties of the canopy, rather than that of the soil [7], can reproduce part of the phase error signature attributed to crops, as does introducing a term linked to the variation of the Normalised Difference Water Index (NDWI) in the decorrelation model [8]. These studies on the effect of crops [6, 8] cover a period of time of one year or less limiting the extraction of recurrent seasonal effects.

The focus of this study is a region around the city of Thessaloniki in Central Macedonia, Greece, where the lowlands are predominantly occupied by agriculture. In order to investigate the long-term and seasonal impact of crops on InSAR phase errors, and to complement existing studies, we compile 5 years of Sentinel-1A/B images [9] with a 6-day recurrence interval. We study the mean InSAR closure phase statistics in relation to coherences, land cover types and the Normalised Difference Vegetation Index (NDVI), and outline spatio-temporal patterns in closure phase over the Thessaloniki plains. While the ultimate objective of distinguishing fading signals from deformation remains unattained, new observations on closure phase and coherence enhance our understanding of the potential origins of these signals.

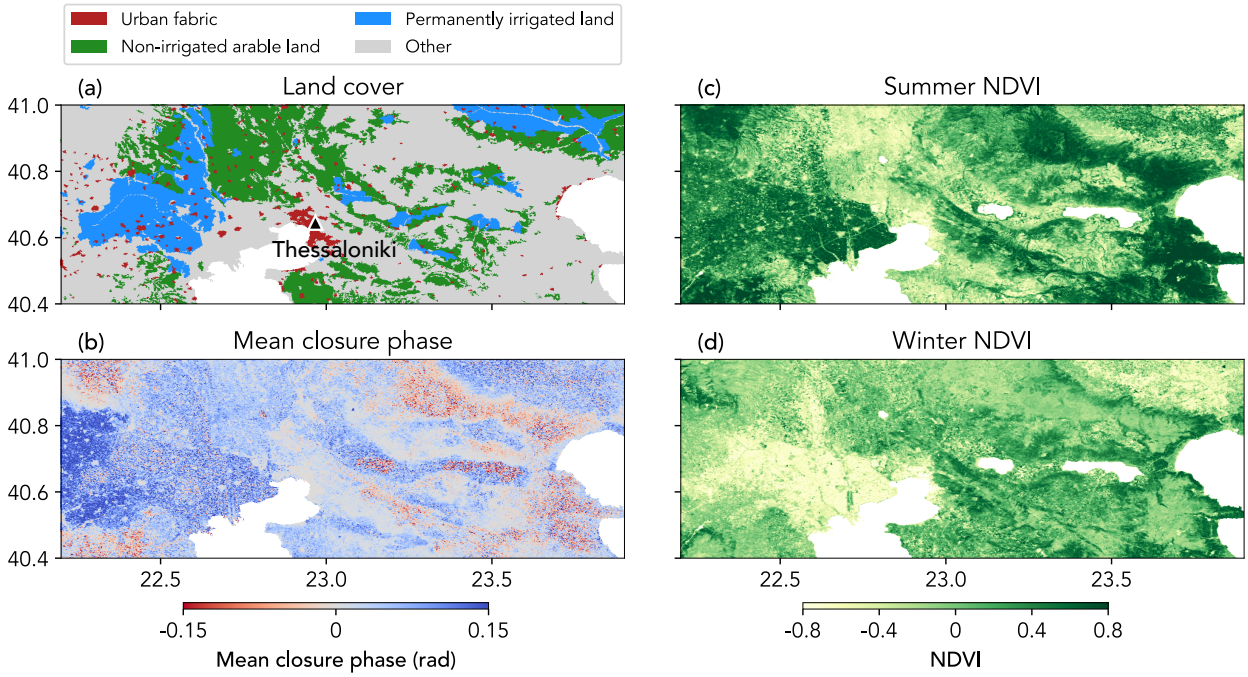


Figure 1 Maps of the Thessaloniki region (a) Land cover map using the classification of [11]. The 'urban fabric' showed here encompasses both discontinuous and continuous classes. (b) Mean closure phase for the whole stack of interferograms. (c) Normalised Difference Vegetation Index (NDVI) for a summer date. (d) NDVI for a winter date.

2 Methods

2.1 Data and processing

We process 292 Sentinel-1 SAR images, from January 2017 to December 2022, from the ascending track 102, with a 6-day revisit period. We build and filter interferograms using ISCE-2 [10] with a small baseline subset (SBAS) strategy, that is we construct all interferograms with temporal baselines inferior to four satellite revisit periods. We multilook the full-resolution interferograms using a window of 14 pixels in azimuth and 70 pixels in range, following a common strategy to improve the signal-to-noise ratio. The resulting multilooked pixels have an approximate ground resolution of 200 metres in azimuth and 160 metres in range. With these wrapped interferograms, we build all possible triplets.

We resample the land covers from the 2018 CORINE Land Cover [11] dataset (**Figure 1a**) on the interferogram grid, attributing the most represented class to each pixel. Out of the 37 classes present on the study zone, we focus on the two predominant crop types: 'permanently irrigated land' and 'non-irrigated arable land'. We also select 'continuous urban fabric' for reference. For the statistical analysis and the timeseries, we randomly select 1,000 pixels per land cover class. The same set of pixels is used for all interferograms.

Sentinel-2 multispectral images are used to compute the Normalised Difference Vegetation Index (NDVI), defined as $\frac{NIR-RED}{NIR+RED}$ with NIR the reflectance of the near infrared band and RED that of the red band. We compute NDVI values for 1 random cloudless image per season for the year 2021 (**Figure 1c, d**).

2.2 Metrics: closure phase and coherence

A full-resolution (SLC) interferogram is constructed by computing the complex conjugate multiplication of two coregistered SAR images z_i and z_j. Multilooking consists in a boxcar spatial averaging of the SLC phase ϕ_{ij} to give a phase $\bar{\phi}_{ij}$. For a closed loop of three multilooked interferograms I_{ij}, I_{jk} and I_{ik}, also called triplet, we define the closure phase as

$$\Psi_{ijk} \equiv \left(\bar{\phi}_{ij} + \bar{\phi}_{jk} - \bar{\phi}_{ik}\right) \bmod 2\pi \tag{1}$$

Its values are wrapped between $-\pi$ and π and are not zero in particular. This operation is a convenient phase calibration, as all the propagative effects, like ground displacement or atmospheric delays, cancel out so that the residual Ψ_{ijk} is the sum of 'inconsistencies' within the three interferograms.

The interferometric coherence γ_{ij} is the normalised correlation between the two coregistered SAR images (z_i and z_j) within a defined spatial window. Here, the coherence is computed between the L single look pixels inside a multilooking window and defined as:

$$\gamma_{ij} = \frac{\left|\sum^{L} z_i z_j^*\right|}{\sqrt{\left(\sum^{L} z_i z_i^*\right)\left(\sum^{L} z_j z_j^*\right)}}. \tag{2}$$

For random, uncorrelated values, the coherence is 0, meaning that the set of pixels gives no interferometric informa-

tion. In contrast, a coherence of 1 indicates strong correlation and meaningful interference. Statistically, the coherence is related to the variance of the closure phase, as demonstrated by analytical [3] and empirical [12] studies: lower values imply greater dispersion of the closure phase.

In the following, we speak about timeseries for variables associated with different time dimensions: the coherence, associated to an interferogram (2 dates), and the closure phase, associated to a triplet (3 dates). For each i^{th} date, we associate the corresponding 6-days-baseline interferogram $\Phi_{i,i+1}$ and coherence $\gamma_{i,i+1}$, when existing, and select the closure phase of the minimal baseline triplet $\Psi_{i,i+1,i+2}$.

3 Results and Discussion

3.1 Non-zero mean closure phase on crops

Figure 1a shows the coverage of the selected classes: non-irrigated and permanently irrigated crops, as well as the urban fabric. **Figure 1b** shows a dominant positive mean closure phase, implying an excess of phase in the selected short-baseline triplets, equivalent to an apparent movement away from the satellite (e.g. subsidence). For all crops, the mean closure phase has a value of about 0.05 rad ($\sim 3°$) for short baseline triplets, implying that the sum of the two 6-day interferograms systematically exceeds the phase of the 12-day return interferogram. This phase excess accumulates over time and will impact the estimated deformation if it is unaccounted for.

Moreover, a delimitation between irrigated land and non-irrigated arable land is visible in the mean closure phase. The mean value is 0.06 rad with a variance of 0.77 rad^2 over irrigated land, compared to a mean of 0.05 rad with a variance of 0.31 rad^2 over non-irrigated land. Therefore, the mean closure phase over irrigated land is more heterogeneous and slightly larger. This contrasts with the urban fabric, which appears to have a zero-mean closure phase, even when situated amongst agricultural land, in line with other studies [12]. The urban fabric thus provides a stable reference for comparison.

To isolate the systematic errors in the closure phase timeseries from the random contributions, we compute the cumulative sum of the closure phase, averaged for each land-cover class. This gives an approximation of the potential error accumulation in the deformation timeseries if the interferometric network consisted of small-baseline interferograms only. Over five years, the cumulative sum on non-irrigated crops shows an increase rate of about 2.8 rad/year (**Figure 2a**), which is roughly equivalent to 1.2 cm/yr in the line-of-sight (LOS) when converted using the Sentinel-1 wavelength. Error accumulates even more rapidly on irrigated crops, with a slope of 3.8 rad/year ($\sim$ 1.7 cm/yr).
The phase accumulation on urban ground is very small but non-zero. Selecting the 'continuous' urban fabric class excludes most large vegetated areas but some parks and trees remain. Furthermore, the spatial averaging of the interferogram and the resulting down-sampling of the land cover map may introduce uncertainty. Nevertheless, we consider continuous urban fabric a reference, as its rate is about 2% of the crop rate. These rates appear to be fairly stable over time, with only small variations, which we discuss in the next section.

3.2 Seasonal variations

In order to observe temporal variations of the growth rate in closure phase accumulation, the mean trend for each land cover is subtracted [13], and the resulting curves are shown on **Figure 2b-d**. Increases are accelerations and decreases are decelerations of the overall accumulation. We compare it to the variations in coherence of the 6-day interferograms and compute the Pearson correlation coefficient.

Both the coherence and the detrended cumulative closure phase show significant seasonality on all croplands (**Figure 2b, c**). Coherence is minimal in the summer and maximal in the winter. The detrended cumulative closure phase tends to shows inverse variations compared to coherence, as confirmed by the negative correlation coefficients (-0.40 and -0.34): more error is accumulated in the summer and deceleration occurs in the winter. In contrast to croplands, urban fabric coherence scarcely shows any seasonality. Although the urban closure phase contains some seasonal contribution, it is much smaller than that observed in cropland areas.

The seasonal signals of irrigated and non-irrigated land differ. The coherence varies, with a larger amplitude on the irrigated land, reaching lower values in summer.
This distinction between irrigated and non-irrigated land is also visible in the NDVI (**Figure 1c, d**), with distinct seasonal patterns. For irrigated crops, the NDVI is very low in winter, suggesting bare soil, and very high in summer, indicating green leaves on the crops. For non-irrigated crops, however, the NDVI is around 0.3 in winter and decreases to around -0.5 in summer. We interpret this as indicating that some non-irrigated crops are planted before winter (reasonably high winter NDVI) and harvested early in summer, or simply dry out during this period (low summer NDVI). The contrast in NDVI variations between summer and winter for permanently irrigated land is consistent with the pronounced seasonal variation in coherence evolution. Additionally, the coherence varies more asymmetrically for non-irrigated land: it increases slower than it decreases, which is not observed for irrigated crops.

Beyond seasonality, local minima in coherence in winter can be associated with snow, which falls more or less every year. The snow cover generally does not last; however, an important snow episode in January 2019 corresponded to a longer local minimum of coherence across all land covers. Furthermore, the correlation coefficient ≥ -0.4 suggests discrepancies in the anticorrelation between the coherence and the detrended cumulative closure phase. For example, the peak in the detrended cumulative closure phase on summer 2020 cannot be explained by an anomaly of coherence. Can we therefore detail the role of coherence in closure phase accumulation, and is a small amount of coherence enough to produce an increase in the cumulative

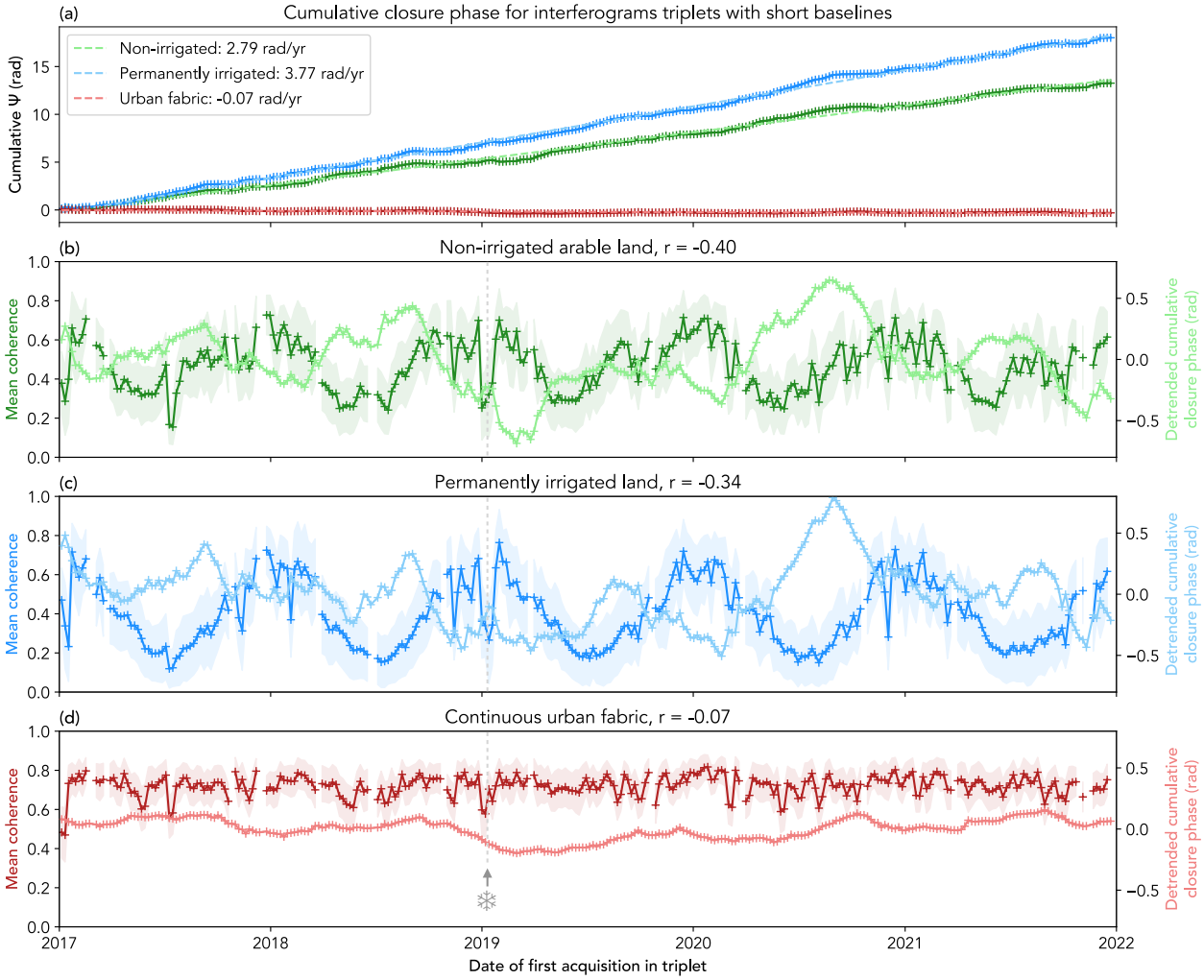


Figure 2 (a) Cumulative sum of the mean closure phases for the series of short baseline triplets, for each class of pixels. The x-axis is the date of the 1st SAR acquisition of the triplet. (b, c, d) Timeseries of the mean coherence for the 6-days interferograms corresponding to each SAR acquisition date, and detrended cumulative closure phase for respectively (b) non-irrigated crops, (c) irrigated crops and (d) continuous urban fabric. r is the Pearson correlation coefficient between the two series. The snowflake shows the snow episode of 2019.

rate of closure phases ?

3.3 The role of coherence

Figure 3 shows the joint distribution of the closure phase and coherence for the three studied cover classes in summer and winter. As expected from the timeseries, the urban fabric displays a similar distribution throughout the year, characterised by high coherence and a closure phase close to zero. In contrast, both cropland categories have very different behaviours in summer and in winter, with a positively biased closure phase affecting pixels of low coherence. Moreover, the lateral spread of closure phase values highlight the expected increase of the variance with decreasing coherence.

Overall, the mean closure phase increases as coherence decreases down to 0.15. For lower coherence values, indicating near-complete decorrelation, the theoretical limit is that the closure phase approaches a random uniform circular variable, with no associated bias. This behaviour is illustrated by irrigated crops in summer, where the point density in low-coherence regions reveals this sharp transition between small non-zero coherences and completely decorrelated data.

When the coherence drops drastically, the single-look interferometric phase within the multilooking window becomes pure random noise. However, this does not preclude continuity of the multilooked phase at lower resolution. It is therefore important to consider the full range of coherence values, especially since **Figure 3** suggests that small but non-zero coherence is associated with larger biases. Conversely, high coherence (> 0.75) appears to guarantee low closure phase variance with a zero mean, as observed in continuous urban areas.

Therefore, we emphasise that only pixels with moderately low coherence are affected by non-zero mean closure phase; however, the converse is not guaranteed. Random processes can reduce coherence to this range without gen-

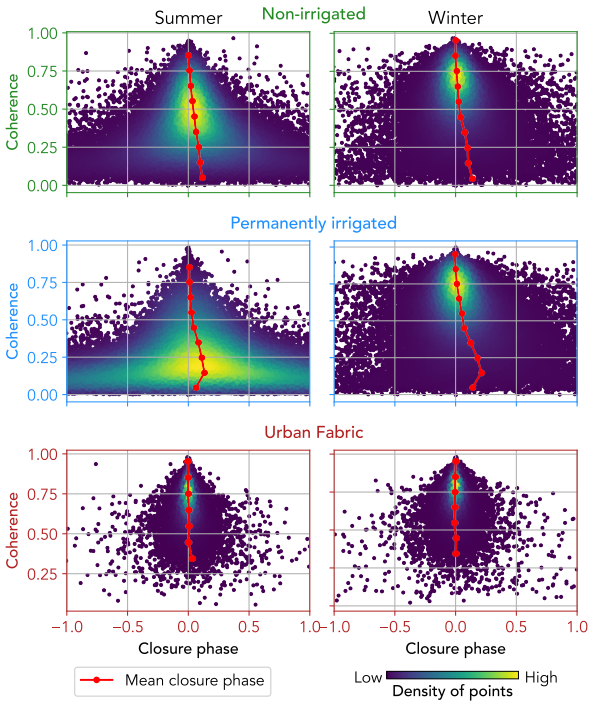


Figure 3 Distribution of the 6-day coherences of each pixel of the selected cover classes in summer and winter, as a function of the closure phase of the minimal baseline triplets built with the interferogram. The mean closure phase for each bin of coherence is represented in red.

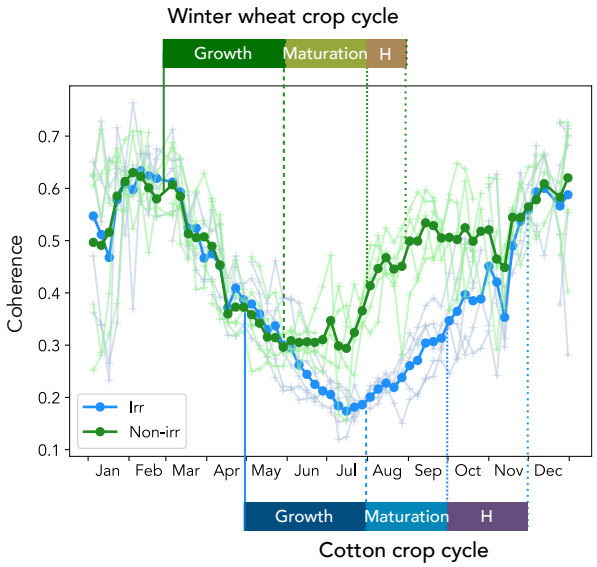


Figure 4 Mean annual coherence, computed on the 5 years of the study, for non-irrigated arable land (in green) and permanently irrigated land (in blue). The actual coherences of each year are plotted behind in lighter colours. The winter-wheat (non-irrigated, in green) and cotton (irrigated, in blue) crop cycles for Greece are shown respectively on the top and the bottom. 'H' is the harvesting phase.

erating excess closure phase [14]. This highlights the need to examine the underlying dephasing mechanisms responsible for both coherence variations and closure phase accumulation.

3.4 Crop growth cycle

Seasonal coherence variations differ between irrigated and non-irrigated crops in two ways. Irrigated crops show a minimum coherence that is delayed (occurring in July instead of May) and larger (falling to less than 0.2 when non-irrigated crops reach 0.33). This pattern aligns with a similar delay in the annual maximum of the closure phase. We attribute these differences to crop types [15], whose growth schedules may require irrigation during the driest summer months (July and August). This interpretation is supported by agricultural statistics for the region.

Using statistics on the land occupation for Central Macedonia [16] over the study period, we estimate that wheat represents about 70% of non-irrigated crops, with most of it likely being winter wheat [17]. In contrast, irrigated crops are more diverse: the dominant crop, cotton, accounts for only 40% of the total. We therefore consider the growth cycles of cotton and winter wheat to be the primary drivers of the observed coherence variations in irrigated and non-irrigated areas, respectively, although other crops are also present in these categories.

Figure 4 shows the mean annual coherence over the 2017-2022 period, highlighting its temporal variation as a function of the month of the year. The crop cycles of cotton and winter wheat are also indicated. Based on crop calendars for Greece [18], we simplify these cycles into three main phases (growth, maturation and harvest) which are expected to coincide with distinct dynamics in terms of backscattering properties.

When comparing the coherence patterns with the crop cycles, we are able to associate variations to corresponding phases, despite the uncertainty surrounding the exact planting and harvest dates. The drop in coherence during the growth phase of both crop types is linked to an increase in the number of scatterers and the development of a skewed velocity profile during stem elongation [6]. The end of the decrease coincides with the start of the maturation phase for both crop types, during which budding, flowering and ripening occur. This corresponds to an increase in coherence for the irrigated areas. In non-irrigated areas, we observe two phases: coherence levels off from early June to mid-July, after which it starts to increase.

Lastly, we would expect decorrelation during harvest but nothing significant is observed in the timeseries. This could be due to the local differences in harvest dates, which would smooth a potential anomaly. It could also be linked to the growth of spring wheat in the region, which is harvested later. In general, comparisons between the crop cycle and our metrics would benefit from field information and more precise calendars.

Consequently, we demonstrated the overall alignment between crop calendars and coherence variations, which seems to be in line with what is qualitatively expected from

plant growth and backscattering effects. Plants will contribute as a temporary scattering mechanism that adds up to the permanent ground scattering, evolving depending on height, density, and probably water content. The anticorrelation of coherence with the detrended cumulative closure phase confirms that plant growth is the relevant process that explains the variations in closure phase accumulation on small-baseline interferograms, in agreement with [3, 6].

4 Conclusions and perspectives

In the Thessaloniki region, the mean closure phase is positive across all crop types. Based on land cover classifications, we distinguish between irrigated and non-irrigated crops and find that phase errors accumulate more rapidly over irrigated areas. We extract a seasonal component in the error signal that is negatively correlated with coherence. While low coherence (< 0.6 and > 0) appears to be a prerequisite for a non-zero mean closure phase, it is not sufficient on its own to explain it. Temporal comparisons between coherence and local crop cycles demonstrate that vegetation growth contributes to the seasonality of the error signal. Notably, a clear contrast between irrigated and non-irrigated areas is observed, consistent with patterns seen in snapshots of the vegetation index (NDVI).
These findings are based on interferograms with short temporal baselines (≤ 12 days), which are generally the most coherent and can be combined through time-series analysis to reconstruct deformation histories. However, our results highlight the need for caution over agricultural areas. The bias affecting deformation time series, resulting from the cumulative non-zero phase error identified here, likely includes both a linear and a seasonal component, which may be misinterpreted as hydrogeological deformation.

In practice, these results support interferometric network selection strategies that explicitly account for the physical origin of the bias in order to minimise its impact. In particular, constructing short-baseline interferograms during periods of limited vegetation growth, especially over irrigated crops, would help mitigate errors. Conversely, lowering coherence thresholds or increasing coherence through strong multilooking may increase the rate of error accumulation over time.

These preliminary results suggest several directions for improvements. Access to more detailed local crop cycle information, typically derived from NDVI timeseries, could provide a clearer picture of its impact on coherence variations and facilitate the selection of optimal acquisition periods when building interferometric networks. The analysis could also be extended to additional land cover classes, such as fruit orchards and olive groves, to provide a more comprehensive view of the interactions between the closure phase and vegetation.

Acknowledgment

We received funding from the INSU PNTS with the project OptInSAR (AAP 2024). Numerical computations were performed on CPUs on the S-CAPAD/DANTE platform, IPGP, France. This publication has been prepared using European Union's Copernicus Land Monitoring Service information (https://doi.org/10.2909/960998c1-1870-4e82-8051-6485205ebbac)

Literature

[1] P. Psimoulis, M. Ghilardi, E. Fouache and S. Stiros, 'Subsidence and evolution of the Thessaloniki Plain, Greece, based on historical leveling and GPS data,' Engineering Geology, vol. 9, pp.55-70, 2007

[2] C. Loupasakis, 'An overview of the land subsidence phenomena occurring in Greece, triggered by the overexploitation of the aquifers for irrigation and mining purposes', Proc. IAHS, 382, pp. 321–326, 2020

[3] F. De Zan, M. Zonno, and P. Lopez-Dekker, "Phase inconsistencies and multiple scattering in SAR interferometry," IEEE Trans. Geosci. Remote Sens., vol. 53, no. 12, pp. 6608–6616, 2015

[4] H. Ansari, F. De Zan, and A. Parizzi, 'Study of systematic bias in measuring surface deformation with SAR interferometry,' IEEE Trans. Geosci. Remote Sens., vol. 59, no. 2, pp. 1285–1301, 2021.

[5] A. Maghsoudi, J. Hooper, T. J. Wright, M. Lazecky, and H. Ansari', 'Characterizing and correcting phase biases in short-term, multilooked interferograms,' RSE, vol. 275, 113022, 2022

[6] Y. Yuan, M. Kleinherenbrink, and P. López-Dekker, 'On Crop Growth and InSAR Closure Phases', IEEE Trans. Geosci. Remote Sensing, vol. 62, pp. 1–12, 2024

[7] M. Nolan, D. R. Fatland, and L. Hinzman, 'DInSAR measurement of soil moisture,' IEEE Trans. Geosci. Remote Sensing, vol. 41, no. 12, pp. 2802-2813, 2003

[8] N. C. Mira, J. Catalão, and G. Nico, 'On the Mitigation of Phase Bias in SAR Interferometry Applications: A New Model Based on NDWI,' IEEE J. Sel. Top. Appl. Earth Obs. Remote Sens., vol. 17, pp. 3850-3859, 2024

[9] EU Copernicus programme. Copernicus Sentinel-1 Data. Available online: https://geodes-portal.cnes.fr/ - (accessed on 13/04/2024).

[10] P. A. Rosen, E. Gurrola, G. F. Sacco and H. Zebker, 'The InSAR scientific computing environment,' *EUSAR 2012*, pp. 730-733, 2012

[11] Corine Land Cover 2018. European Union's Copernicus Land Monitoring Service information, Available online: https://land.copernicus.eu/en/products/corine-land-cover/clc2018- (accessed on 12/06/2025)

[12] M. Dalaison, B. Pinel-Puysségur, R. Jolivet, B. Raimbault, and L. Drique 'Relationship between closure phase error and interferometric coherence in multilooked InSAR' AGU Fall Meeting, G34A-08, 2024

[13] E. Wig, R. Michaelides, and H. Zebker,'Fine-resolution measurement of soil moisture from cumulative InSAR closure phase' IEEE Trans. Geosci. Remote Sensing, vol. 62, pp. 1-15, 2024.

[14] F. De Zan, F. Rocca, A. Ferretti, P. Lopez-Dekker and M. Eineder 'Comments on "Influence of the Statistical Properties of Phase and Intensity on Closure Phase"', IEEE Trans. Geosci. Remote Sensing, vol. 59, no. 7, pp. 6277-6278, 2021

[15] A. Villarroya-Carpio, J. Lopez-Sanchez and M. Engdahl, 'Sentinel-1 interferometric coherence as a vegetation index for agriculture,' RSE, vol. 280, 113208, 2022

[16] Hellenic Statistical Authority. Agricultural Areas and Production. Available online: https://www.statistics.gr/en/statistics/-/publication/SPG06/- (accessed on 15/09/2025).

[17] A.S. Lithourgidis, C.A. Damalas and A.A. Gagianas, 'Long-term yield patterns for continuous winter wheat cropping in northern Greece,' European J. of Agronomy, vol. 25, no. 3, pp 208-214, 2006

[18] USDA Foreign Agricultural Service. International Production Assessment Division. Available online: https://ipad.fas.usda.gov/cropexplorer/- (accessed on 15/09/2025)